Eur. Phys. J. D **9**, 111–117 (1999)

THE EUROPEAN PHYSICAL JOURNAL D

EDP Sciences

Frequencies, times, and forces in the dynamics of Na clusters

P.-G. Reinhard[1], M. Brack[2], F. Calvayrac[3], C. Kohl[4], S. Kümmel[3], E. Suraud[3], and C.A. Ullrich[5]

[1] Institut für Theoretische Physik, Universität Erlangen, Staudtstrasse 7, D-91058 Erlangen, Germany
[2] Institute for Theoretical Physics, University of Regensburg, D-93040 Regensburg, Germany
[3] Laboratoire de Physique Quantique, Université Paul Sabatier, 118 Route de Narbonne, F-31062 Toulouse Cedex, France
[4] Institute for Nuclear Theory, University of Washington, Seattle, WA 98195, USA
[5] Department of Physics, University of Missouri, Columbia, MO 65211, USA

Received: 1 September 1998 / Received in final form: 22 November 1998

Abstract. Laser excitation of metal clusters depends on various parameters such as frequency, intensity, and pulse time. We give here an overview of relevant time scales and forces for the example of Na clusters. Variation of laser intensity is studied in connection with second harmonic generation. We see a rather sudden transition from a perturbative regime at low intensities to a field-dominated regime for larger intensities. We use the non-linearized time-dependent local density approximation (TDLDA), together with a local pseudopotential for the interaction of the valence electrons with the ions. Explicit ionic motion is taken into account in one test case where we demonstrate the importance of ionic effects for the detailed time evolution at times larger than 100 fs.

PACS. 36.40.-c Atomic and molecular clusters – 36.40.Gk Plasma and collective effects in clusters – 71.24.+q Electronic structure of clusters and nanoparticles – 72.20.Ht High field and nonlinear effects

1 Introduction

The dynamical response of the valence electron cloud in metal clusters has been a much studied topic over the past two decades. Earlier studies have been concerned with the response in the linear domain and associated spectral properties of clusters; for reviews see, e.g., [1–3]. New experimental developments, such as collisions with energetic ions [4] or irradiation by intense femtosecond laser pulses [5, 6], have paved the path to the non-linear regime. At the same time, the theoretical description in terms of the full-fledged non-linearized time-dependent local density approximation (TDLDA) has been established [7–9]. The early theoretical work has been concerned mainly with general spectral properties. Electron emission, which plays a crucial role at strong excitations, has been studied subsequently [10, 11] for the case of fast (and thus rather simple) excitation mechanisms by energetic ions. A much more complex, but also much richer, world of variants opens up when laser excitations in the non-linear regime are considered, because there are more parameters to be tuned: the frequency, the intensity, and the pulse profile. There already exist a few first attempts to explore this rich field theoretically (see [12, 13] for clusters and [14] for atoms in strong laser pulses). It is the aim of this contribution to continue these considerations of cluster dynamics in intense laser fields, trying to sort the various scales of frequencies, times, as well as forces with an emphasis on variation of the laser intensity (i.e. the external force). Furthermore, we will take into account here the detailed ionic structure. This has become feasible with the recent development of a simple, namely local, pseudo-potential which provides reliable dynamical properties, see [15, 16]. Moreover, we will also briefly address the interplay of laser excitation with explicit ionic dynamics, again continuing a previous first exploration of coupled electronic and ionic dynamics [17].

The paper is organized as follows. Section 2 contains a short explanation of the formal background (TDLDA, pseudopotentials). In Sect. 3, we discuss the various time scales and the forces involved in cluster dynamics. In Sect. 4, we study systematic variation of laser intensity considering second harmonic generation (SHG) in $Na_9{}^+$ as a test case. And in Sect. 5, we demonstrate the importance of ionic motion in excitations which run over longer times.

2 Formal framework

The electronic dynamics is described through the time-dependent Kohn–Sham equations within the non-linearized TDLDA using the exchange-correlation functional of [18]; for further details of our treatment see [9, 12]. In oder to simplify the calculations and to allow a widespread variation of parameters, we impose axial symmetry on the electronic densities and mean fields. This constitutes the dynamical generalization of the cylindrically averaged pseudo-potential scheme (CAPS) [19]; it is a valid approximation for the test case of this paper, $Na_9{}^+$, whose CAPS

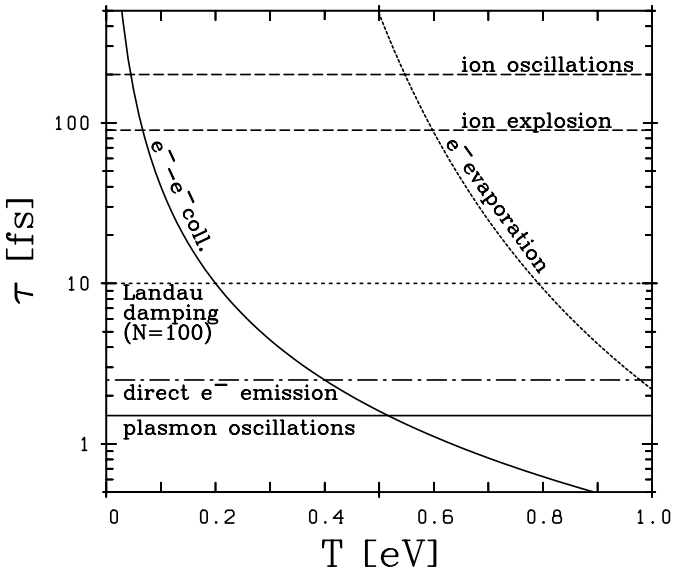

Fig. 1. Schematic view of times scales involved in the dynamics of Na clusters, drawn as function of temperature T.

ground state has the configuration "144": a ring of 4 electrons, followed by another ring of 4 electrons (twisted by 45° with respect to the first ring), and topped by one single ion on the symmetry axis.

For the pseudopotential we use the newly constructed local form $V_{\rm Gauss}(r) = -Ze^2/r \sum_i c_i \mathrm{erf}\left(r/(\sigma_i\sqrt{2})\right)$, with $\mathrm{erf}(x) = \frac{2}{\sqrt{\pi}} \int_0^x dy\, \exp(-y^2)$, $\sigma_1 = 0.681\,\mathrm{a_0}$, $\sigma_2 = 1.163\,\mathrm{a_0}$, $c_1 = -2.292$, and $c_1 = 3.292$; for the details of its construction, see [15, 16]. This potential provides reliable spectral properties as seen, e.g., in the spectrum of Na_9^+ in Fig. 3 below. The ionic structure has, of course, been reoptimized in connection with the new pseudopotential.

As dynamical observables we will consider the dipole power spectrum and the number of escaped electrons $N_{\rm esc}$. The power spectrum is constructed by recording the dipole moment $D(t)$, Fourier transforming it to $\tilde{D}(\omega)$, and finally forming $\mathcal{P} = |\tilde{D}(\omega)|^2$. In turn, $N_{\rm esc}$ is determined by computing the number of electrons inside an analyzing sphere of $16\,\mathrm{a_0}$ (note that the cluster radius is $8\,\mathrm{a_0}$), and building the complement to the initial electron number N. Further observables are the strength of SHG, derived from the power spectrum, and the ionic positions (which are trivially given).

3 Orders of magnitude

Various time scales compete in the dynamics of metals. We try to visualize them for the case of Na clusters in Fig. 1. The fastest time is set by the period of the plasmon oscillations. Immediately following is the time needed for direct electron emission, which is induced directly by the force pulse from the external field plus amplification through the plasmon response. About one order of magnitude later, there comes Landau damping which is caused by coupling of the Mie plasmon mode to nearby particle-hole ($1ph$) states. The corresponding relaxation time depends very much on the actual system. For singly charged Na clusters, a maximum is found in the range $N \approx 100 - 1000$ [20]. A typical value is 10 fs which corresponds, e.g., to the spectral width of the dipole response in a Na cluster with $N \approx 100$. These three times – plasmon period, emission time, and Landau damping – depend only weakly on the temperature of the system, which is indicated by drawing straight horizontal lines in Fig. 1.

Electron-electron collisions provide a further dissipative mechanism. They transport excitation energy from the $1ph$ modes to $2ph$ and higher configurations. The collision rate is largely suppressed at low excitation energies due to Pauli blocking of the final scattering states. The relaxation times from collisions thus depend strongly on temperature. In a semiclassical evaluation one finds for Na clusters $\tau_{\rm col}^{-1} = 0.4\,T^2 \mathrm{fs}^{-1}\mathrm{eV}^{-2}$ Note that the TDLDA does not account for damping through electron-electron collisions, but it does include Landau damping. In view of the strongly different time scales ($\tau_{\rm col} \gg \tau_{\rm Landau}$ for small temperatures), the TDLDA thus constitutes a good approximation for our purposes.

Once the system has gained internal energy, thermal electron evaporation sets in. Its time scale can be computed using the Weisskopf estimate [22], as indicated in Fig. 1. One sees that it usually shows up far beyond any other mechanism, but it can become competitive for very high temperatures.

There are two aspects to the time scales for ionic motion. Ionic vibrations are nearly always present, associated with a period of about 200 fs. The excitation mechanism can introduce other time scales. For instance, very energetic excitations can ionize the cluster quickly into a high charge state, such that the strong Coulomb force drives an explosion whose speed depends on the degree of ionization. For example, ionizing Na_{12}^{+++} with a short laser pulse yields significant ionic effects already at ~ 100 fs [17].

All times shown in Fig. 1 need to be related to the time scale of the excitation process. The situation is rather simple for fast ionic collisions, which are completed before any one of the constituents of the cluster can react. Laser excitations, ranging nowadays down to 20 fs, provide a much wider choice of time profiles which all interfere with several of the internal cluster processes. This gives rise to a rich variety of dynamical processes, most of which have yet to be explored.

Typical energies and forces are visualized for the example of a Na_9^+ cluster in Fig. 2. The uppermost panel shows the stationary Kohn–Sham potential along the z axis, calculated in the jellium model (using a soft Woods-Saxon profile for the ionic density with $r_s = 4\,\mathrm{a_0}$ and surface width $1\,\mathrm{a_0}$). The two occupied single-electron states are indicated by horizontal lines. The energy difference for the Mie plasmon excitation is shown by the vertical arrow. It is obvious that it remains far below ionization threshold for this cluster. The middle panel shows the result from using detailed ionic structure with the local pseudopotential as sketched in Sect. 2. The huge repulsive spike comes from the one ion sitting directly on the z axis. This demonstrates the enormous fluctuations caused by the ionic po-

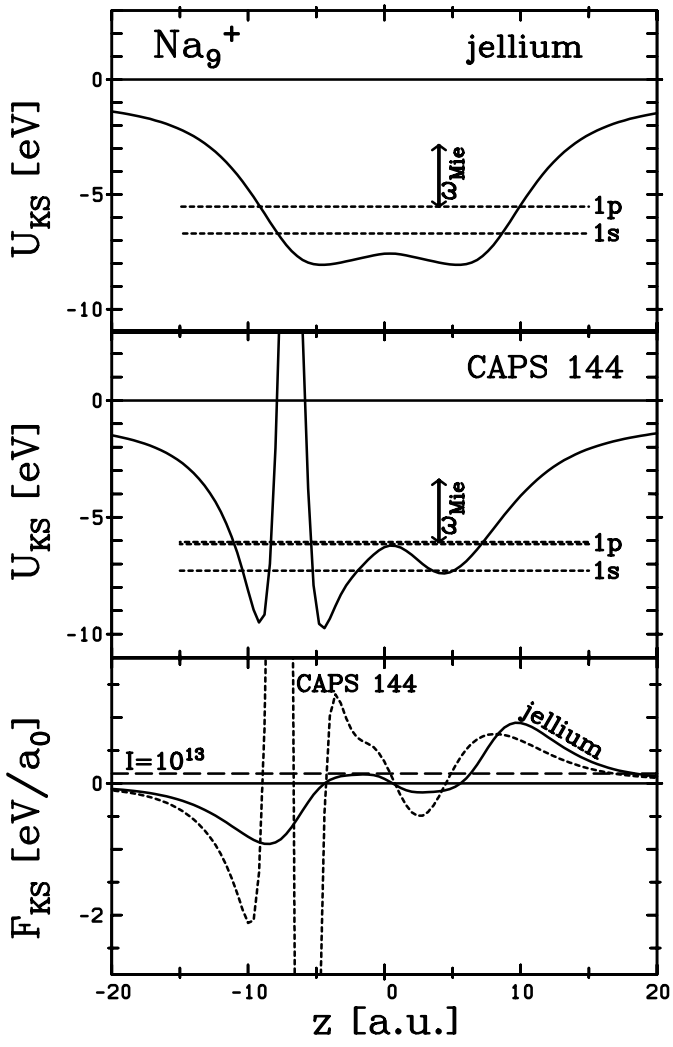

Fig. 2. Potentials and forces in the $Na_9{}^+$ cluster. Top: Static Kohn–Sham potential along the z axis for the case of soft jellium background, together with the position of the occupied single electron states as indicated and the energy of one Mie plasmon. Middle: As upper part, but with full ionic structure in the CAPS configuration "144". Bottom: Forces from the above potentials for jellium (full) and ionic background (dotted) as indicated. The force from a strong laser beam with intensity $I = 10^{13}\,\mathrm{W/cm^2}$ is indicated by a dashed line.

tentials. But the quantum-mechanical electronic wavefunctions do not resolve all these spatial details. They explore basically an averaged potential which, after all, is not so much different from the jellium potential. One may note a slightly stronger binding of the single electron states, which is a welcome effect because the soft jellium model notoriously underestimates the ionization threshold. The model with detailed ionic structure performs much better in that respect.

The lower panel of Fig. 2 shows the forces as derived from the Kohn–Sham potentials above. The ionic peak yields, of course, huge spikes in the force. But they are confined to a very small volume in space such that the net effect remains moderate. More important is the broad force peak at the boundaries of the cluster which appears in the jellium model as well. This peak characterizes the binding forces for the valence electrons in the cluster.

The interplay between binding forces and the external perturbing force is decisive for the dynamical regime. For small perturbations, we stay in a regime where the frequency of the laser determines the transitions and where photons are absorbed adiabatically one after another. This regime is well described by (higher-order) perturbation theory [23]. For large perturbations, we come into a regime which can be called "field dominated", where amplitudes are more important than frequency and photon number and ionization through suppression of the Coulomb barrier may become significant (see, e.g., the Keldysh theory of ionization [24]). "Small" and "large" depends upon the relation between binding force and perturbation. The latter should be viewed as an effective perturbing force, composed by the external force plus possible field amplification through resonant processes [13]. To give an example, we have in Fig. 2 drawn the external force corresponding to a laser pulse with intensity $I = 10^{13}\,\mathrm{W/cm^2}$. Adopting an amplification factor of about $2-3$, we come already in conflict with the binding forces and, indeed, we will see in the next section that this is the intensity where we certainly are beyond the perturbative regime.

4 Variation of laser intensity

Laser beams offer many parameters to be varied. Variation of the freqency is the basic tool to explore spectra, e.g., in laser absorption experiments. Variation of the pulse length accesses very different dynamical regimes, as shown experimentally in [6] and demonstrated schematically in Fig. 1 (and discussed to more extent in [25]). Often,one even shapes the pulse profile, which is an important tool in fs laser spectroscopy. Here we will concentrate on the variation of the intensity for the particular case of SHG as an example. As a test case, we take free $Na_9{}^+$ with full ionic structure in the CAPS configuration "144". It is to be noted that actual experiments are performed for large clusters attached to a surface [26]. The surface induces a common orientation of the clusters. This provides coherent amplification of the signal and enhances the symmetry breaking, which is the necessary condition for coupling to the second harmonics. The free $Na_9{}^+$ cluster already shows some symmetry breaking in the ground state (with an octupole moment of $\beta_3 = 0.15$), which suffices for being a probe in our schematic exploration. (Note that attachment to a NaCl surface enhances, indeed, the octupole moment by a factor of two [27]; but we prefer to skip the complications due to the surface for the present study.)

The laser frequency has an influence on the efficiency of the SHG. With a schematic analytical model, we find that best conditions exist if the plasmon resonance is involved on one side of the process, either for the impinging laser pulse or for the emerging second harmonic. There is

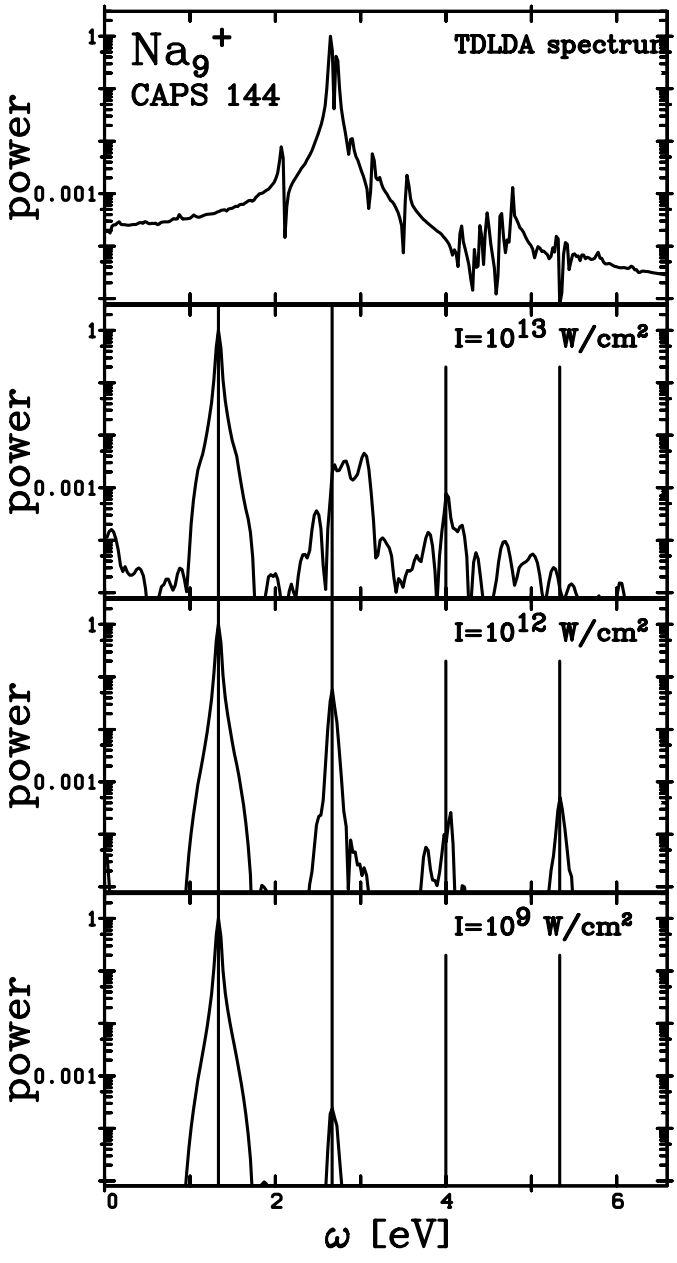

Fig. 3. Second harmonic generation on $Na_9{}^+$ with full ionic structure in CAPS configuration "144". The lower three panels show the dipole power spectra from excitation with a laser at half Mie resonance frequency, i.e. 1.33 eV, and with pulse of length 145 fs for various laser intensities as indicated. The uppermost panel shows the excitation spectrum in the linear regime.

a slight preference for the latter due to better suppression of background noise. We thus choose a laser field with half the resonance freqency, corresponding to ω=1.33 eV in the present test case. The pulse length determines the spectral selectivity. We choose here a trapezoidal pulse with length $T_{\rm pulse}$=145 fs and 10% switching time at each end. The pulse covers about 100 plasmon periods, providing sufficient spectral resolution for our purposes. We keep the ionic positions frozen during that time, although this may become inappropriate for the more energetic excitations. But we aim at disentangling the influences, and study the ionic motion separately in the next section. What remains is the variation of the laser intensity which will be studied here. The procedure is straightforward. We solve the Kohn–Sham equations within TDLDA in the presence of the laser field and extract the power spectrum as well as the number of escaped electrons in the manner explained above.

Figure 3 shows the resulting power spectra for three intensities. The upper panel is the power spectrum from an instantaneous initial excitation and serves to give information on the excitation spectrum of the cluster as such [9]. The spectrum shows the clear dominance of the Mie plasmon peak with a faint $1ph$ splitting (already an effect of ionic structure and absent in the simple jellium model).

The strength of SHG depends strongly on the laser intensity, as can be seen from the dramatic increase of the SHG signal between the lowest panel and the one above it. This is no surprise, because the SHG in the perturbative regime (here requiring, of course, second-order perturbation theory) should grow with the square of the field strength, and thus should be proportional to I. The higher harmonics grow even faster and become nicely visible in the more intense case of $I = 10^{12}\,\mathrm{W/cm^2}$. But this is already at the limits of the perturbative regime. At ten times higher intensity (next higher panel), the wanted signal is destroyed. Here we have clearly entered the field-dominated regime where superposition occurs between the laser frequency and the strong field fluctuations coming from competing processes, here mostly from electron emission.

A summary of the trends with intensity is shown in Fig. 4. The lowest panel shows a schematic comparison of the competing forces. The external force is, of course, a straight line with slope 1/2. The dotted lines indicate the effective perturbing forces which emerge together with the electronic response. Two cases are shown, one for a laser beam in resonance with the Mie plasmon and another one for a laser below resonance which still shows substantial amplification. It is this off-resonant case which applies for the laser beam used here. One sees that the effective force crosses the binding force (denoted "g.s. binding") just at $I = 10^{12}$–$10^{13}\,\mathrm{W/cm^2}$ which we found to be a critical value in the previous figure. It is to be noted that this critical value applies for the frequency below resonance. It may become even lower for a resonant case. The further limits in this plot are the force of the naked ion configuration ("last valence") and the binding force for the core electrons ("core binding") which both come into play for intensities $I{>}10^{15}\,\mathrm{W/cm^2}$. This shows that the regime where field dominance can be studied in Na clusters corresponds to a rather narrow window of intensities.

The second panel from below shows the number of directly emitted electrons. There is obviously a sharp transition around this critical $I = 10^{12}\,\mathrm{W/cm^2}$ (note that this is stretched by the logarithmic plotting). Below we are in the perturbative regime where electron escape proceeds $\propto I^\nu$ as a ν-photon process [12]. Above, we are soon in a situ-

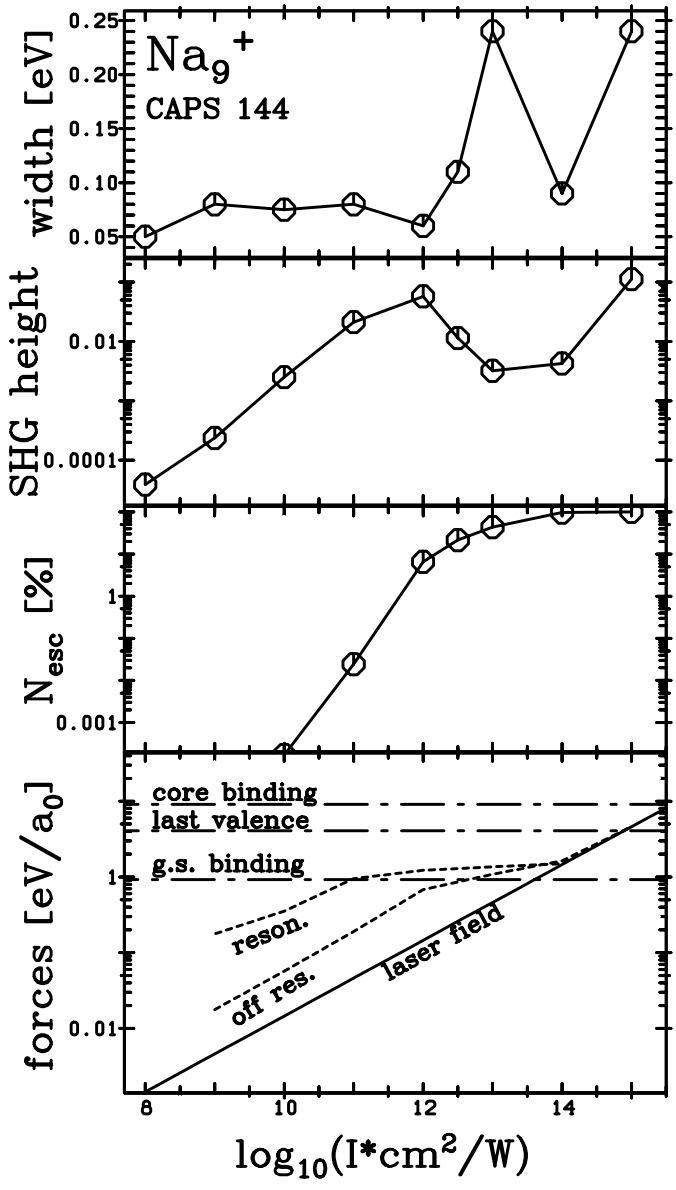

Fig. 4. Summary of results from SHG on $Na_9{}^+$ with full ionic structure in CAPS configuration "144", drawn versus intensity of the exciting laser beam. Bottom: Schematic view of the various forces on the electrons. The force from the laser field grows $\propto \sqrt{I}$. The actual force on the valence electrons is amplified by electronic response and shown for two typical cases, on and off the Mie resonance. The limits for binding in the ground state of $Na_9{}^+$ and full ionization ("last valence") are indicated as well as the binding force of the nearest core electrons. Second from below: Number of escaped electrons $N_{\rm esc}$. Second from above: Height of the peak in the second harmonics relative to the leading peak at the laser frequency. Top: Width (FWHM) of the peak in the second harmonics.

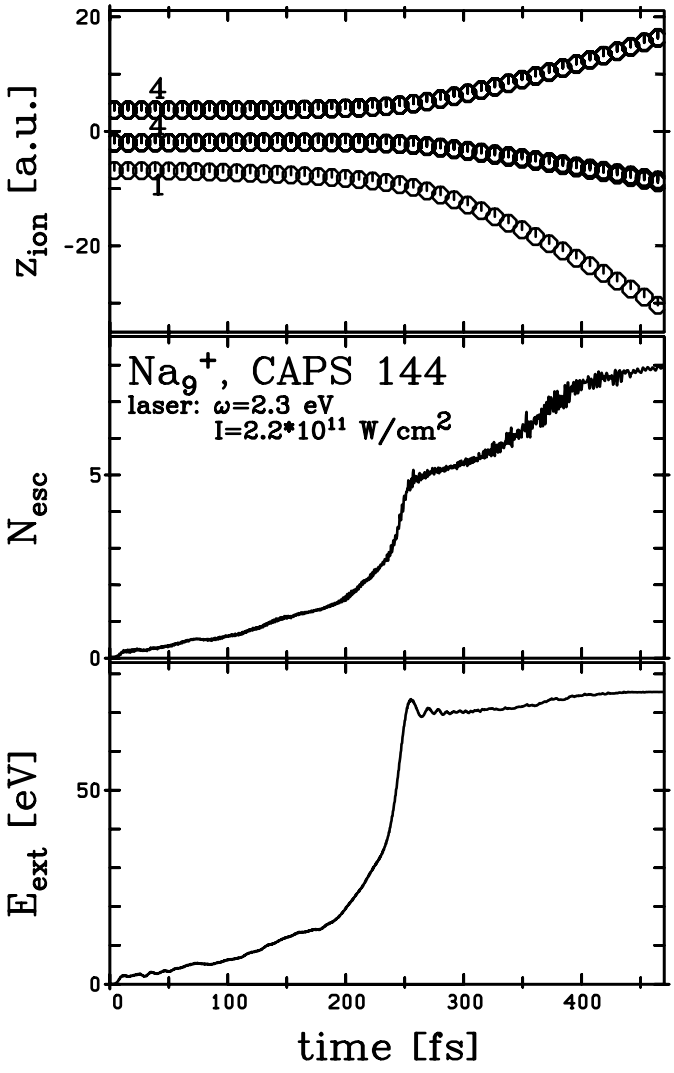

Fig. 5. Time evolution of ionic structure and electronic key observables for $Na_9{}^+$ in a laser field with intensity $I = 2.2\times 10^{11}\,\mathrm{W/cm^2}$ and frequency $\omega = 2.3\,\mathrm{eV}$. Top: The z positions of the 9 ions with multiplicity (arrangement in rings according to CAPS) as indicated. Middle: Number of escaped electrons $N_{\rm esc}$. Bottom: Energy $E_{\rm ext}$ absorbed by the cluster from the external laser field.

ation where nearly all valence electrons are stripped off and very little is left for SHG. The second panel from above shows the height of the SHG peak in the power spectrum relative to the base harmonic peak. One sees the steady growth with intensity up to $I = 10^{11}\,\mathrm{W/cm^2}$. The next step already hints at a reduced growth, and after that the signal breaks down. Corroborating information is provided by the width (FWHM) of the SHG peak, shown in the uppermost panel. It stays at a low level (basically representing the resolution of our analysis) up to the critical intensity, and jumps to a regime of large and fluctuating values for high intensities.

5 Interplay with ionic motion

Up to now, we have kept the ions frozen during the analysis of the electronic dynamics. This is certainly not perfectly valid once we enter the field-dominated regime

where a strong ionization destabilizes the given ionic configuration. Ionic motion changes the resonance conditions which, in turn, has a large impact on the dynamical evolution. Experimental hints on such effects can be found in [28]. These experiments have, however, been done with Pt clusters which are presently too hard to handle with our tools. We give here an analogous example for Na clusters. Starting point is again Na_9^+ in the CAPS configuration "144". It is excited by a "subcritical" laser field below resonance ($I = 2.2\times10^{11}\,\mathrm{W/cm^2}$ and $\omega = 2.3\,\mathrm{eV}$) with a very long pulse. We use techniques to solve the coupled ionic and electronic equations of motion as explained in [17]. The results are shown in Fig. 5. Initially, very little happens. One sees a slow growth of ionization (middle panel), associated with a slow absorption of external energy E_{ext} from the beam (lower panel). This causes a slow elongation of the ionic configuration due to the repulsive Coulomb force (which first tries to enhance the quadrupole moment). The elongation lowers the plasmon peak, and at around 250 fs the electron cloud comes into resonance with the laser beam. The effect is dramatic. One sees a sudden increase in the absorbed energy (lower panel), a large portion of which is converted into direct electron emission. This enhances the degree of ionization which, in turn, boosts a Coulomb explosion of the whole cluster. This all happens in a very short period of less than 10 fs. After that, the energy absorption levels off; there is some delayed electron emission (probably thermal evaporation from the very hot cluster, see Fig. 1), and the ions separate on a rather fast scale. This example proceeds in a particularly dramatic fashion, by virtue of the chosen conditions. Other cases may evolve more gently. But also more violent cases are conceivable. In any case, one sees that ionic motion should be considered when stepping beyond 50−100 fs.

6 Conclusions

Various dynamical regimes of the dynamics of Na clusters are accessed when considering laser excitation over a broad range of the experimental parameters. After a short overview of the relevant time scales, we have concentrated on force scales in relation to the external force (or intensity) of the laser. This has been exemplified for SHG on a small Na cluster as a test case. For low intensities with $I \leq 10^{11}\,\mathrm{W/cm^2}$, one stays in the perturbative regime where good estimates can safely be computed from linear response, or appropriate higher-order perturbation theory for multi-photon processes. Above that, there is a rather sudden transition into a field-dominated regime where amplitudes or forces become more important than frequencies. For the theoretical description, this requires large-amplitude techniques such as the non-linearized TDLDA.

The transition shows up in the particular case of the SHG as a sudden spectral destruction of the SHG signal. The best yield is achieved shortly before the transition. It is thus worthwhile to evaluate this critical point more systematically for other sizes and materials.

The field-dominated regime lasts for about $2-3$ orders of magnitude of intensity. The physics of the valence electron cloud becomes obsolete for larger intensities $I \geq 10^{15}\,\mathrm{W/cm^2}$.

Finally, we have studied how the ionic motion changes the resonance conditions. It becomes effective when sufficient ionization (around 20% in the present test case) triggers a large drift of the ions which then change the plasmon position substantially. Dramatic consequences emerge if the plasmon comes into resonance with the laser field. The interplay of the various parameters (frequency, intensity, pulse length, cluster size, material) opens a rich field of phenomena from which we have here only shown a first exploratory example. It will become an area of intense investigations in the near future.

This work has been supported by the French-German exchange program PROCOPE 95073, the Institut Universitaire de France, and the Deutsche Forschungsgemeinschaft. Two of the authors (P.-G. R. and E. S.) thank the Institute for Nuclear Theory (Seattle) for its hospitality, financial support and computational facilities. Furthermore, inspiring discussions with G.F. Bertsch, C. Guet, H. Haberland, J. Köhn, and K.H. Meiwes-Broer are gratefully acknowledged.

References

1. W. de Heer: Rev. Mod. Phys. **65**, 611 (1993)
2. M. Brack: Rev. Mod. Phys. **65**, 677 (1993)
3. U. Kreibig, M. Vollmer: *Optical Properties of Metal Clusters* (Springer, Berlin 1995)
4. F. Chandezon *et al.*: Phys. Rev. Lett. **74**, 3784 (1995)
5. T. Baumert, G. Gerber: Adv. At. Mol. Opt. Phys. **35**, 163 (1995)
6. R. Schlipper, R. Kusche, B. von Issendorff, H. Haberland: Phys. Rev. Lett. **80**, 1194 (1998)
7. F. Calvayrac, E. Suraud, P.-G. Reinhard: Phys. Rev. B **52**, 17056 (1995)
8. K. Yabana, G.F. Bertsch: Phys. Rev. B **54**, 4484 (1996)
9. F. Calvayrac, E. Suraud, P.-G. Reinhard: Ann. Phys. (N.Y.) **255**, 125 (1997)
10. C.A. Ullrich, P.-G. Reinhard, E. Suraud: Phys. Rev. A **57**, 1938 (1998)
11. P.-G. Reinhard, E. Suraud, C.A. Ullrich: Eur. Phys. J. D **1**, 303 (1998)
12. C.A. Ullrich, P.-G. Reinhard, E. Suraud: J. Phys. B **30**, 5043 (1997); *ibid.* **31**, 1871 (1998)
13. P.-G. Reinhard, E. Suraud: Eur. Phys. J. D **1**, 303 (1998)
14. C.A. Ullrich, E.K.U. Gross: Comments At. Mol. Phys. **33**, 211 (1997)
15. S. Kümmel, M. Brack, P.-G. Reinhard: Phys. Rev. B **58**, 1774 (1998)
16. S. Kümmel *et al.*: Eur. Phys. J. D (1999), these proceedings
17. F. Calvayrac, P.-G. Reinhard, E. Suraud: J. Phys. B **31**, 5023 (1998)
18. J.P. Perdew, Y. Wang: Phys. Rev. B **45**, 13244 (1992)

19. B. Montag, P.-G. Reinhard: Z. Phys. D **33**, 265 (1995)
20. J. Babst, P.-G. Reinhard: Z. Phys. D **42**, 209 (1997)
21. A. Domps, E. Suraud, P.-G. Reinhard: Phys. Rev. Lett. **81**, 5524 (1998)
22. V. Weisskopf: Phys. Rev. **52**, 295 (1937)
23. F.H.M. Faisal: *Theory of Multiphoton Processes* (Plenum Press, New York 1987)
24. L.V. Keldysh: Zh. Eksp. Teor. Fiz. **47**, 1945 (1964) [Sov. Phys. JETP **20**, 1307 (1965)]; M.J. DeWitt, R.J. Levis: J. Chem. Phys. **108**, 7739 (1988)
25. C.A. Ullrich, P.-G. Reinhard, E. Suraud: Eur. Phys. J. D (1999), these proceedings
26. A. Assion, B. Lang, M. Simon, S. Voll, F. Traeger, G. Gerber: Chem. Phys. Lett. **296**, 579 (1998)
27. C. Kohl, P.-G. Reinhard: Z. Phys. D **39**, 605 (1997)
28. L. Köller, M. Schumacher, J. Köhn, S. Teuber, J. Tiggesbäumker, K.-H. Meiwes-Broer: Phys. Rev. Lett. **82**, 3783 (1999)